MARCEL DEKKER, INC. • 270 MADISON AVENUE • NEW YORK, NY 10016

DRUG DEVELOPMENT AND INDUSTRIAL PHARMACY
Vol. 28, No. 9, pp. 1059–1076, 2002

RESEARCH PAPER

Wet Film Dimensions of Capsule Walls During Dip Coating

Colin M. Keary[1,*] and William A. Heeschen[2]

[1]*The Dow Chemical Company, Larkin Laboratory, Midland, MI 48674*
[2]*The Dow Chemical Company, Analytical Laboratory, 1897 Building, Midland, MI 48674*

ABSTRACT

The objective of the present study was to improve our understanding of the relationships between wet film dimensions, dip sequences, and the physicochemical properties of the dip solutions as they pertain to the dip-coating process for the manufacture of hard-shell capsules. To achieve this objective, it was necessary to develop a technique to quantify wet film dimensions. A further objective was to develop a predictive model for dip coating with hydroxypropyl methylcellulose (HPMC) solutions. It is hoped that the information contained in this article on significant variables controlling wet film thickness will help manufacturers develop consistent manufacturing controls and processes.

INTRODUCTION

Details of the development and technology of two-piece, hard-shell capsules are conveniently summarized in a monograph[1] published by The Pharmaceutical Society of Great Britain. When one considers the crucial role of the dipping process in the preparation of capsules, it is surprising that the monograph offers little by way of relating the dip process to capsule dimensions.

Capsule-making practices that worked for gelatin have been modified, by capsule makers, to be applicable to hydroxypropyl methylcellulose (HPMC) and other polymers. Capsules are available in a variety of sizes to accommodate various size doses of ingredients and to meet consumer preferences. Commercially, capsule caps and bodies are separated, filled, and re-assembled in high-speed filling machines. Dimensional and geometrical tolerances in filling machines are extremely narrow, and

*Corresponding author. Fax: (989) 638-9838; E-mail: cmkeary@dow.com

DOI: 10.1081/DDC-120014574
0363-9045 (Print); 1520-5762 (Online)

www.dekker.com

unattended operation is commonly demanded. Consequently, the capsules themselves must be manufactured to precise tolerances.

MANUFACTURING PROCESS

To the best of our knowledge, most current production of HPMC capsules is performed on modified gelatin capsule machines. Modifications are necessary as a consequence of the inherent differences in the thermal behavior of gelatin solutions and HPMC solutions. The most concise statement of these differences is: "gelatin solutions gel upon cooling, whereas HPMC solutions gel upon heating." Both polymers have the ability to form films when their gels or solutions are dried.

A typical gelatin capsule machine is approximately 30 ft long, by 6 ft wide, by 8 ft high. Capsules are formed in a dip-coating process in which steel molds of caps and bodies are dipped into a solution of polymer for the purpose of depositing onto the outer surface of the molds a thin coating of polymer gel and solution that may be converted into solid film upon drying. Dry films are then stripped from the molds, trimmed to length, and caps and bodies are assembled prior to ejection of capsules from the machine. From there, the capsules proceed to quality control, printing, and packaging, as appropriate.

Great effort is expended throughout the whole process to avoid defects; it is remarkable how many significant defects have been categorized by the industry.[1] It is even more remarkable how qualitative the understanding is concerning the source and remedy of most of the defects.

Molds are essentially cylindrical in shape, but they do have a slight taper toward their dome end. In addition, capsule manufacturers have a variety of methods of mechanically locking caps to bodies and these methods are molded into the film by the inclusion of precisely located notches and grooves on the molds. Various additional grooves or rings may be added to increase stiffness or circularity according to the preferences of the manufacturer.[2]

Most machines have been customized to some extent according to the preferences of the capsule maker. The capsule molds, commonly called "pins," are mounted in a row on a bar. Body pins are mounted on one set of bars and cap pins on other bars. The capsule machine is effectively divided lengthwise, with caps on one side and bodies on the other side. Both types of bars pass through the process in phase with each other, and caps and bodies are manipulated to arrive facing each other to allow for assembly as unsealed capsules.

Figure 1 illustrates one possible complex dip sequence. Note that a silhouette of a capsule body pin has been included in the figure to illustrate a qualitative relationship between speeds and position on the pin. Note that this withdrawal involves four speeds, whereas the insertion is a single, high speed.

Capsule makers place tremendous dependence on the readings from simple viscometers that dip into the polymer solutions in the dip tanks. Fortunately, the shear dependence of the viscosity of simple HPMC solutions, of the type and concentrations used in the present process, is essentially newtonian at 30°C,[3] but this behavior cannot be assumed to persist for more complex formulations.

DIP COATING THEORY

In a review of the physics of various coating techniques, Scriven[4] wrote: "Dip coating is a simple old way of depositing onto a substrate, especially small slabs and cylinders, a uniform thin film of liquid for solidification into a coating. The basic flow is steady, and in it film thickness is set by the competition among viscous force, capillary (surface tension) force and gravity. Thickness and uniformity can be sensitive to flow conditions in the liquid bath and gas overhead. The faster the substrate is withdrawn, the thicker the film deposited. This can be countered by using volatile solutes and combining rapid enough drying with the basic liquid flow. Then the physics grows more complicated, theoretical prediction of process performance more difficult, and control of the process more demanding. Outside of R&D labs it is far less often used in precision coating manufacture than a variety of premetered coating methods."

Apparently, Scriven excluded capsule manufacture from his definition of "precision coating manufacture." Perhaps this exclusion is justified on the basis that, in the case of capsules, the "coating" is removed from the substrate. In his review,[4] all of the presented theory of dip coating pertained to coating with low viscosity solutions.

Dip coating glass by a sol–gel process has been studied extensively[4–7] because of the commercial

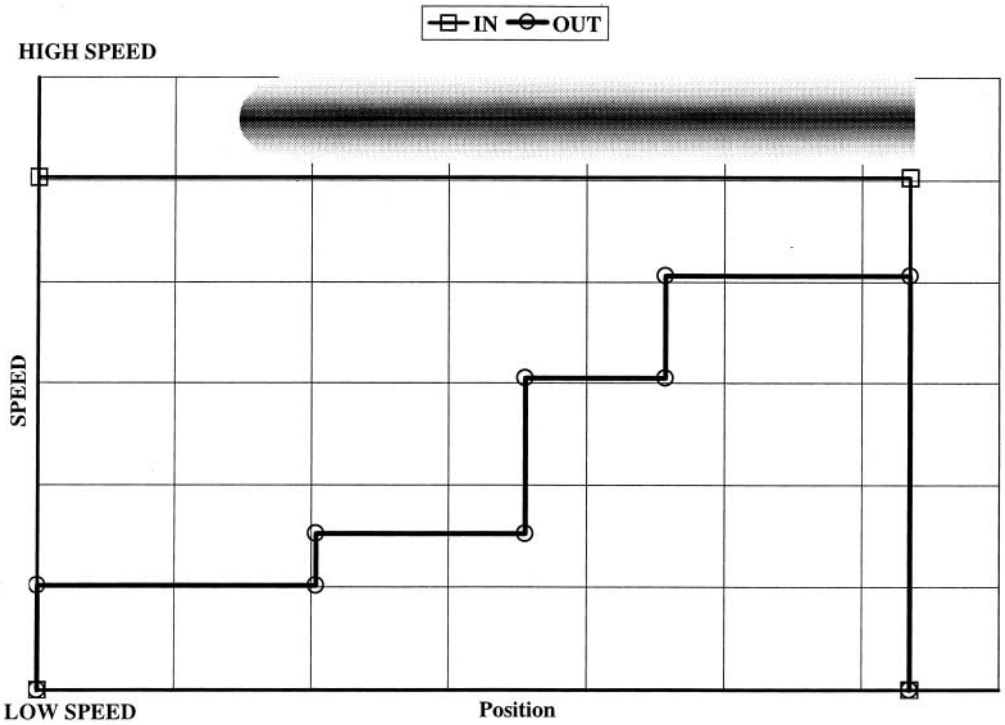

Figure 1. Typical dipping sequence.

importance of the process for optical applications. This is representative of the majority of published literature on the theory of dip coating; restricted to the use of low viscosity, newtonian liquids.[8,9] There are comparatively few published studies concerning non-newtonian liquids,[10,11] and no publications have been found that involved thermally-induced rheological modifications such as occur in capsule manufacture.

NEWTONIAN LIQUIDS

For the purpose of evaluating the predictive capacity of existing[5,6] theories of dip coating, let us temporarily ignore the non-newtonian aspects of HPMC thermal gelation. Consider only the dimensions of a size "0" capsule body, and follow an evaluation that is analogous to a sol–gel evaluation.[5] Table 1 shows typical inputs and simple volume–weight–area calculations. Resulting wet and dry film calculations are illustrated in Table 2. An examination of Tables 1 and 2 shows that the ratio of wet film thickness to dry film thickness is approximately 5. It was specified in Table 1 that the wall thickness of the capsule was 0.0104 cm, and the calculations in Table 2 predict that a wet film thickness of 0.052 cm would be required, assuming complete densification during the wet-to-dry transformation. This assumption may be varied to accommodate various drying levels or the presence of additives. In comparison, Sarkar[3] reported that the wet-to-dry film thickness ratio for capsules should be in the range 8–12; no details of his calculations were given to support these values.

INFLUENCE OF PROCESS PARAMETERS ON WET FILM THICKNESS

In addition to predicting dry film thickness from wet film thickness, the literature[4–6] contains some studies of the influence of process parameters on the wet film thickness. It is instructive to consider Fig. 2, that illustrates two systems representing withdrawal of a continuous substrate from a bulk liquid[7,9] and withdrawal of a batch substrate from a bulk liquid.[12] The main difference between these two cases is seen in the location of the zone where the film achieves constant thickness. In the batch process,

Table 1

Dip Coating Volume–Weight–Area Calculations

		Symbol		Units
Input	Body length	L	1.8520	cm
Input	External diameter	d	0.7340	cm
Input	Wall thickness	t_D	0.0104	cm
Input	Moisture	m	5.00	%
Input	Concentration of HPMC solution	C_M	20.00	%
Input	Density of HPMC	ρ_M	1.2600	g/cm^3
Input	Density of solvent	ρ_S	1.0000	g/cm^3
	External area of cylinder: $2\pi rh = 2\pi(d/2)(L - d/2)$	A_{cyl}	3.4243	cm^2
	External area of hemisphere: $2\pi(d/2)^2$	A_{dome}	0.8463	cm^2
	External area of body: $A_{cyl} + A_{dome}$	A	4.2706	cm^2
	Volume of film: At_D	V_f	0.0444	cm^3
	Weight, including moisture: $V_f\,[(100 - m/100)\rho_M + (m/100)\rho_S]$		0.0554	g

Table 2

Calculation of Wet:Dry Film Ratio

	Calculation			
To achieve	DRY FILM THICKNESS =	t_D	0.0104	cm
	Film density: $(100 - m/100)\rho_M + (m/100)\rho_S$	ρ_P	1.2470	g/cm^3
	Solution density: $(C_M/100)\rho_M + (100 - C_M/100)\rho_S$	ρ	1.0520	g/cm^3
	Ratio of densities: $(\rho - \rho_S)/(\rho_M - \rho_S)$	F_ρ	0.2000	
Requires	WET FILM THICKNESS $= t_D/F_\rho =$	t_W	0.0520	cm
Ratio	t_W:t_D		5.00	

constant thickness occurs somewhere close to the surface of the bulk liquid and thickness falls to zero at the leading edge. In the continuous process, where there is effectively no "leading edge," constant thickness is achieved above a dynamic meniscus region. Dip coating a long length of fiber might be considered "continuous," whereas dip coating a capsule is clearly a "batch" process. Both of the systems in Fig. 2 involve removal of the substrate at constant speed. Neither system contains any concept of an insertion stage; the profiles that have been shown are a snap-shot at a time when the liquid is moving downwards and the substrate is moving upwards.

MATHEMATICAL DESCRIPTION OF DIP COATING WITH LOW VISCOSITY LIQUIDS

Scriven[4] has identified several forces that compete and contribute variously to the wet film thickness, h, e.g.:

- Viscous drag on the liquid upwards by the rising substrate, proportional to liquid viscosity, μ, and withdrawal speed, U.
- The force of gravity, g, on any species adhering to the withdrawing substrate, proportional to liquid density, ρ.

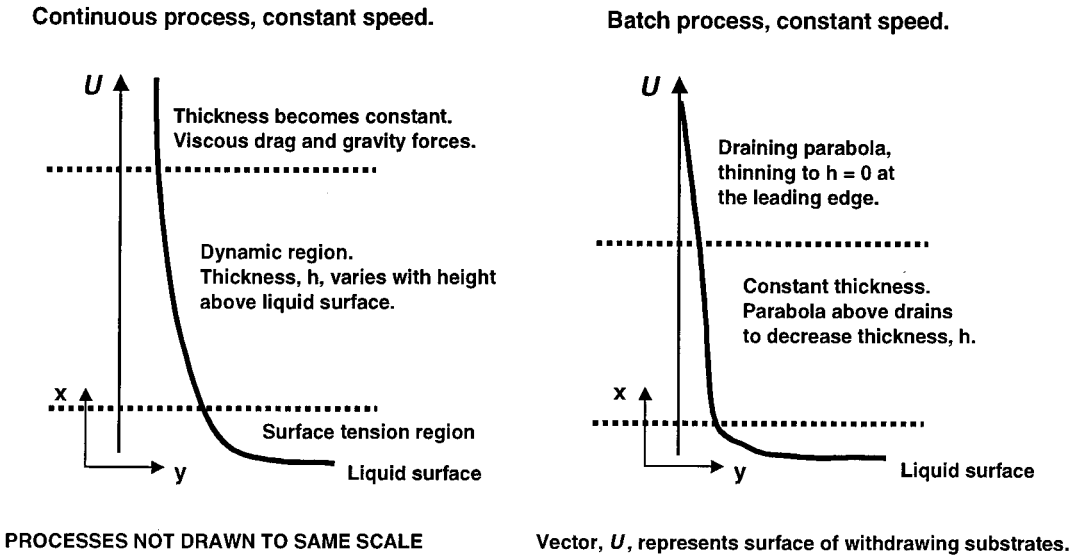

Figure 2. Profiles of low viscosity liquids on vertical, moving surfaces.

- Forces arising from surface tension at the substrate–liquid meniscus.

In most instances, with low viscosity liquids, the wet film thickness, h, is realized where viscous drag and gravity are in balance:

$$\text{Drag force} \propto \mu U/h$$

$$\text{Gravity force} \propto \rho g h$$

$$\therefore h = c_1\sqrt{\frac{\mu U}{\rho g}} \tag{1}$$

where c_1 is a proportionality constant around 0.8 for newtonian liquids.[4] Equation (1) states that film thickness increases as viscosity increases and as withdrawal speed increases, and also states that film thickness decreases as wet film density increases. It must be emphasized that the insertion part of the stroke does not feature in the equation unless μ is somehow modified by the insertion process, and the modified value is implied in the equation.

As the substrate starts to withdraw in any low viscosity batch process (see the "batch" part of Fig. 2), liquid drains from the leading edge and this edge may become very thin. Away from the leading edge, viscous drag is opposed by gravity, but complete equilibrium might never be achieved in any given batch process, and any one of the interacting forces might dominate the whole system, depending upon the particular properties of the batch process. If, however, forces attain equilibrium, then it is predicted that the balance between upward-acting and downward-acting forces will be adequately described by those equations that were developed for continuous dip coating.

Let x be the distance downward from the leading edge, then a draining film with a parabolic thickness profile, h, that diminishes to zero at the leading edge has been described[12]:

$$h = \sqrt{\frac{\mu x}{\rho g t}} \tag{2}$$

where t is the time since the leading edge left the surface of the dip tank. Equation (2) predicts that in a batch dipping process, with low viscosity liquid, the wet film thickness increases at increasing distance from the leading edge and decreases with time. The net result of these opposing effects is that a batch process may reach the same constant film thickness as could be achieved in a continuous process at x_c, where h reaches the steady-state thickness as given in Eq. (1).

At sufficiently low withdrawal speeds, in continuous processing, Eq. (1) must be modified to account for the significant contribution of surface tension, σ; the modified equation is[4]:

$$h = 0.944\left(\frac{\mu U}{\sigma}\right)^{1/6}\left(\frac{\mu U}{\rho g}\right)^{1/2} \quad (3)$$

which is found to be useful when $\mu U/\sigma$ (the capillary number) is less than 10^{-2}.

Returning to Eq. (3), as the film changes thickness, the location[4] of any given thickness, h, moves down the substrate at a speed, v_h, proportional to h^2, as can be seen in Eq. (4):

$$V_h = \frac{\rho g}{\mu} h^2 \quad (4)$$

The parabolic profile reaches constant thickness at $Ut - x_c$, where U is the speed of withdrawal and t is the time since the leading edge left the dip tank. As a consequence of drainage, the parabolic profile lengthens in such a way that the end effect occupies a fixed fraction of the withdrawn length.

The best way to illustrate these various phenomena is by replicating here the example given by Scriven.[4] When a substrate is withdrawn at $U = 2.5$ mm/sec from liquid of surface tension $\sigma =$ 25 dyne/cm, viscosity $\mu = 1$ cp, and density $\rho = 1$ g/cm^3, the capillary number is 10^{-4} and, from Eq. (3), the steady-state film thickness, h, is 3.3 μm and extends 96% of the way to the leading edge. When withdrawal is halted, the continuing drainage extends the parabolic profile downward, increasing the distance x_c at a speed that is 4.1% of U, according to Eq. (4).

For comparison, making capsules with HPMC might involve the following parameters: multiple withdrawal speeds within a single stroke (see Fig. 1), liquid of surface tension of approximately 55 dyne/cm, liquid that undergoes surface gelation, viscosity $\mu =$ 1000–5000 cp, and density $\rho = 1.0$–1.2 g/cm^3.

DIP COATING WITH HPMC

The film profile given in Fig. 3 is a prediction of relevant aspects of dip coating a hot pin with a HPMC solution. Figure 3 is also a snap-shot of the profile that adheres to the pin as the liquid moves down and the pin moves up; but the main differences from Fig. 2 are that withdrawal speed is not constant and two additional "zones" have been added. Zone 1 is created during the insertion stage by thermal gelation and zone 2 may or may not be created during the withdrawal stage by further thermal gelation. Figure 3 does not imply that the boundaries of zones 1 and 2 are parallel to the pin wall, nor is it implied that the zones are of known geometry. It is not proposed that there is clear demarcation between zone 1 and zone 2, or between zone 2 and the adhering liquid HPMC.

EXPERIMENTAL DETAILS OF THE DIPPING SIMULATOR

The complexity of the thermal response of HPMC solutions is well known.[14,15] It was decided to develop an experimental technique to measure wet film dimensions in real time. The technique was based upon image analysis of digital video recordings of dipping sequences as performed on a "dipping simulator." To avoid problems of maintaining focus on a moving pin, it was decided to simulate capsule dipping by raising and lowering the dip solution in relation to a fixed pin at the camera's focal point.

An apparatus was built to manipulate pins and HPMC solution while making digital video recordings of the process. The apparatus included a series of manually controlled, linear slides to allow precise x–y–z motion of the camera mount. A heated, rotating assembly was provided to hold the pins. A stepper motor and screw-driven slide allowed vertical movement of a vial filled with HPMC solution.

- Camera was a Sony XC-75CE, CCD black-and-white video camera module with 752×582 pixels.
- Lens was a Navitar Zoom 7000, Macro Zoom 18–108 mm F/2.5.
- Vertical motion of the dip solution was performed with a NEMA Type 23 stepper motor (Velmex Inc., Slo-Syn M061, 60 oz-in holding torque) driving a linear slide (Velmex Inc., MB2506P10J-S2.5). This combination provided 0.00635 mm per step resolution.
- Stepper motor was controlled via a Velmex NF90-2 programmable controller, with a resolution of 400 steps per revolution.
- Commands were entered to the controller via an RS-232-C interface from a PowerMac 7100/66 operating with Mac OS8.
- Video movies were stored on Syquest Sy-Jet 1.5 GB cartridges.
- Apparatus control and image analysis was done with the NIH Image software, version

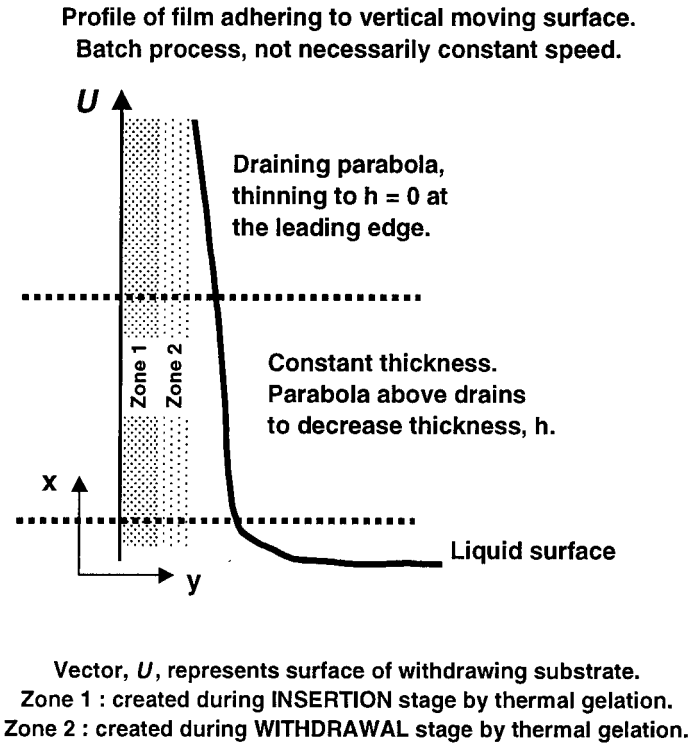

Figure 3. Proposed profile of thermally gelling system on vertical, moving, heated surface.

1.61 (NIH Image was written at the National Institutes of Health and is in the public domain. The program and documentation is available via the Internet at http://rsb.info.nih.gov/nih-image.) Custom-written NIH Image macros for automation of the dipping process, movie set-up and collection, image analysis, and data reduction and storage were written by the authors.

- For photography, the dipping process was back-lit with a fluorescent light box, fitted with a diffuser cover, masked as necessary. Room illumination was turned off during photography and reflective surfaces were covered with black card.

Polystyrene vials (37 mL) were used as dip tanks and HPMC solution was added to vials until the solution meniscus exceeded the vial rim. No cooling of these dip tanks was provided; a fresh vial and solution were used for each dip to limit surface gelation and heating of the bulk solution.

The rotor of the apparatus was designed to enable the pin to remain in the camera's field of vision after rotation through 180°. The apparatus was equipped with an etched foil element, silicone rubber heater (Watlow Electric Manufacturing Co., # F010050C7, 5″ × 1″, 120 V, 50 W) to provide heat in an attempt to simulate the large thermal mass of pin bars. Pins were heated in an oven prior to loading into the rotor and were equipped with an axial hole to accommodate a type-J, flexible, thermocouple. Power to the heater was controlled with a variable powerstat and entered the heater via a rotating contact (Mercotac Inc., #205). Pins were held by a spring-loaded, slide-in mount. The simulator pins were designed to have as large a contact area as possible with the heated surface of the pin holder. In addition, this contact area was cupped in the pin direction to capture any HPMC that might run down the pin if rotated into the dome-up position. Pins of several different diameters were made to span the range of common capsule sizes. Note that these pins were parallel-

sided and did not contain any notches or rings, unlike production pins.

A glance at Fig. 1, for example, shows the demands that are placed on stepper motor control of the dipping sequence.

A commonly used dip sequence within this study is shown in Fig. 4, illustrating one of the NIH Image screens. Row-by-row, this sequence performs the following tasks (**bold** text items refer to the "Action" column of Fig. 4):

- Set the **in**itial **gap** to 2 mm between dome of pin and liquid meniscus, close 2 mm gap at a speed of 12 mm/sec, set cumulative time = 0.0 sec.
- **In**sert pin into liquid to a depth of 20 mm at a rate of 20 mm/sec, this takes 1 sec, cumulative time = 1.0 sec.
- **Pause** creates a delay step of 0.2 sec, cumulative time = 1.2 sec.
- Start video recording of the **movie**.
- Withdraw by traveling **out** at 20 mm/sec for 18 mm, this takes 0.9 sec, cumulative time = 2.1 sec.
- Withdraw the remaining 2 mm of the **out** stroke at a rate of 5 mm/sec, this takes 0.4 sec, cumulative time = 2.5 sec.
- Travel to the fully **out gap** of 57 mm at a rate of 12 mm/sec; this is an artifact of the simulator. In production, at this stage the pin bars would begin to travel upwards, away from the dip tanks, rotate into a dome-up position, and be accumulated in the upper deck for travel along the length of the heating zones.

AUTOMATED IMAGE ANALYSES: TERMINOLOGY AND CONVENTIONS

The video system was used as a recording, optical micrometer. Images were rotated 90° clockwise, so that withdrawal of a pin from the liquid surface appeared as a horizontal movement on the computer screen. An image of the bare pin, recorded immediately prior to dipping, was recorded and then "subtracted" electronically from each frame of the video that recorded the withdrawal process. This is illustrated in the montages, shown in Fig. 5, from actual video recording taken with the equipment described above. The left-hand column shows images of an unheated, back-lit pin emerging from the surface of the liquid; from top to bottom, the frame numbers were 2, 5, 10, and 20. Frames were recorded every 0.5 sec; so that these frame numbers represent 1, 2.5, 5, and 10 sec, respectively, from the time that the pin started the withdrawal stage. Recall that in this simulator the dip vessel moves downward while the pin remains stationary. Due to this, frame 2 of the left-hand column of Fig. 5 is partially obscured by the vessel; the vessel has only traveled downwards 20 mm and the surface of the liquid in the vessel is clearly seen where the material

Report for 20%_6.35 pin_70C_.25 Delay

20 frames, 0.5000 seconds between frames.
Scale = 29.6063 pix/mm.
Frame size = 23.2383 mm wide X 10.8085 mm high.

Profile:

Action	Rate	Travel	Time	EndPos	RunTime
InGap	12.00	2.00	0.2	0.0	0.0
In	20.00	20.00	1.0	20.0	1.0
Pause	0.00	0.00	0.2	20.0	1.2
Movie	0.00	0.00	0.0	20.0	1.2
Out	20.00	-18.00	0.9	2.0	2.1
Out	5.00	-2.00	0.4	0.0	2.5
OutGap	12.00	-57.00	4.8	-57.0	7.3
FlpDly	0.00	0.00	1.0	-57.0	8.3
FlpTim	0.00	0.00	0.0	-57.0	8.3

Figure 4. Complexity of dipping sequence.

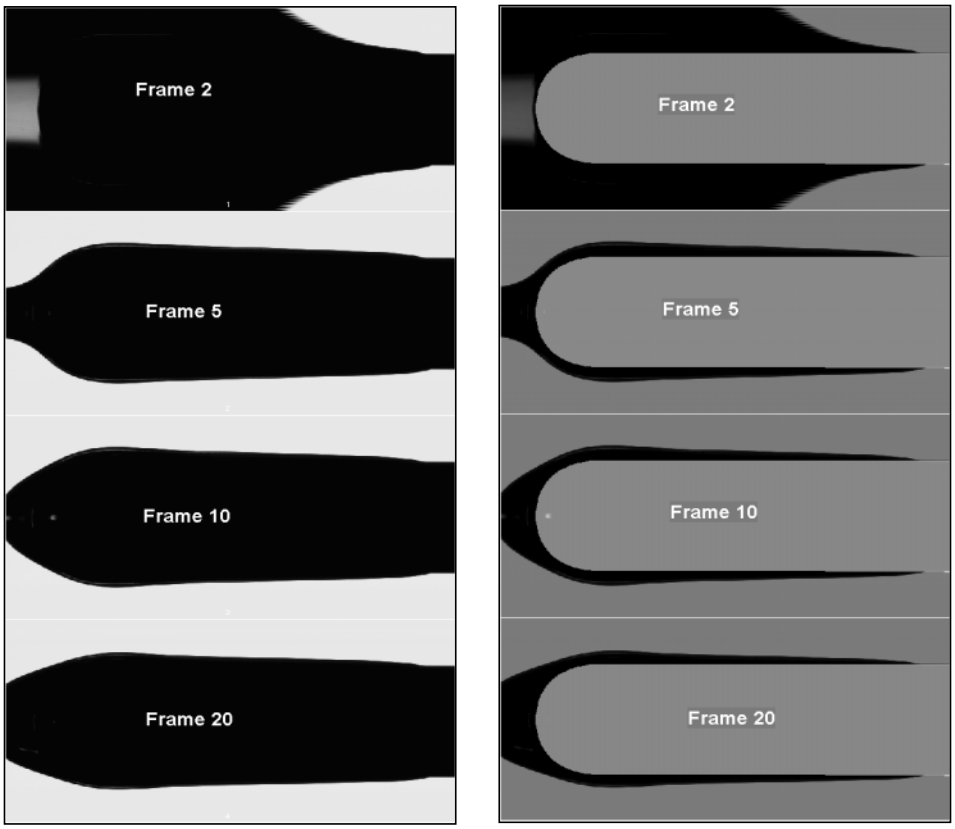

Figure 5. Montage of video frames and electronic subtraction of bare pin.

that adheres to the pin meets the surface of the liquid in the vessel. By the time that frame 5 was captured, the downward moving vessel has cleared the video window and exists beyond the left-hand edge of the frame.

The right-hand column of Fig. 5 illustrates the on-screen, visual results of electronic subtraction of the unheated, bare pin from the left-hand column images. Frame 2 in the right-hand column of Fig. 5 clearly shows the spatial relationships of the pin, dipping vessel, material adhering to the pin, and the leading edge of the adhering layer. Frames 5, 10, and 20 show that there is a thick layer of liquid at the dome end of the pins. Comparison of frame 5 with frame 20 reveals that liquid drainage has taken place from the viscously-adhering layer on the walls of the pin toward the dome end of the pin. This has resulted in a thinning of the pin coating and a thickening of the liquid area at the dome end of the pin.

NIH Image macros performed dimensional analyses on the "subtracted" images, as illustrated in Fig. 6 and Table 3. Toward the bottom of Fig. 6, the term "ROI" has been added. This is the "Region Of Interest" that defines the width of the active video window. Dimensions in the "Y" direction are not lengths along the pin, nor are they lengths of dipped pin; they are lengths along the ROI. This is significant because we have to expose a portion of the pin beyond the maximum dip depth to allow for scale calibration and to allow us to view the leading edge of the wet film.

Figure 6 is, effectively, a cross-section through the coated pin; measurements of the film thickness on both sides of the pin were performed every 0.25 mm in the "Y" direction. However, it is apparent that the leading edge does not start at the same "Y" value for both sides of the pin. This is typically an indication that the pin was not perfectly vertical in relation to the surface of the liquid. Table 3 lists the first 13 rows of a multi-page analysis of a typical subtracted image; all dimensions are given in millimeters. The first row gives column headings X, Y

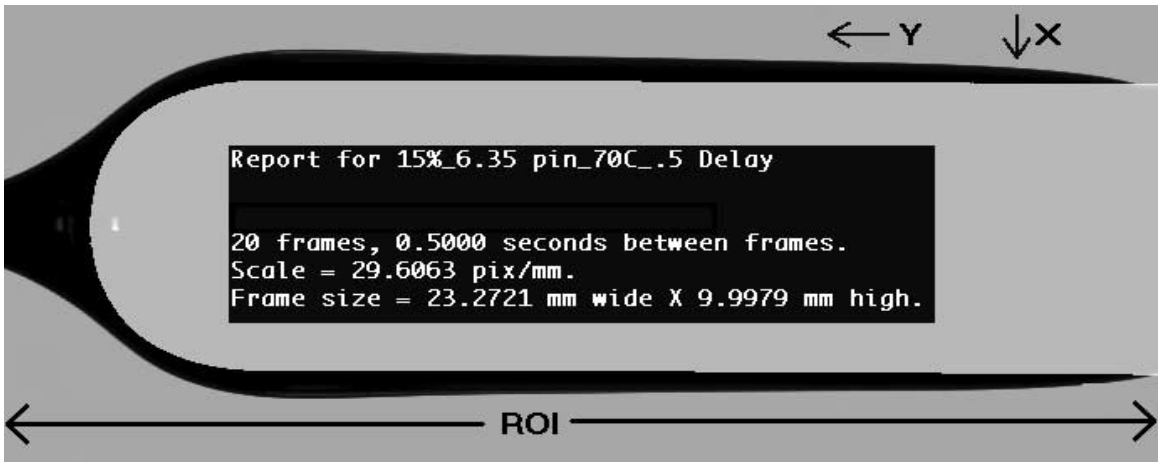

Figure 6. Close-up of subtracted image.

Table 3

NIH Image Macro Analysis of Subtracted Image

	X	Y	Length
1	8.106	0.507	0.105
2	1.655	0.777	0.105
3	8.14	0.777	0.173
4	1.638	1.047	0.139
5	8.157	1.047	0.207
6	1.621	1.317	0.173
7	8.174	1.317	0.241
8	1.587	1.587	0.241
9	8.174	1.587	0.241
10	1.571	1.858	0.274
11	8.191	1.858	0.274

and Length; the latter refers to the thickness of the wet film. By 1.587 mm in the "Y" direction, both sides of the pin were equally thick (length = 0.241 mm).

Image Resolution of Dimensions

Assuming the ability to resolve images to 1 pixel, we have a resolution of approximately 34 μm per pixel, at the magnification that was selected, i.e., 29 pixels per millimeter in Fig. 6. This magnification represents a practical dynamic range of the camera/pin/screen combination. In all of the experiments, the diameter of the pin was known accurately and was used to set the scale for NIH Image. The dynamic range was determined by those lens settings at which the whole of the dip depth could be accommodated in a single screen width; this avoided the complexity of finding relative locations of higher magnification images that were split over more than one screen width. In other words, resolution was dictated by the need to accommodate a convenient ROI.

Image Resolution of Time

All video movies were recorded at two frames per second; the system was capable of >30 frames per second. By experiment, it was determined that no change in film dimensions could be detected within 0.5 sec of any normal event. Most movies lasted 10 sec, which provided 20 frames to cover the withdrawal step of the process. In manufacturing operations, the dome end of the pins will typically have cleared the surface of the liquid within 5 sec of the start of withdrawal, see Fig. 1.

Non-thermally Gelling Systems

A systematic evaluation of significant parameters was undertaken and it was decided to consider how non-gelling systems behaved before proceeding to thermally gelling systems. Room-temperature pins were dipped into HPMC solutions and measurements were performed with the video system.

To evaluate the precision and reproducibility of the techniques, a pin (6.35 mm in diameter) was inserted at 20 mm/sec and withdrawn at 5 mm/sec from vials of HPMC solutions (15%). Designated as "Experiment #3," this was replicated sixfold and the

results are shown in Fig. 7. Every 2 mm along the ROI, text boxes list the mean and standard deviation of the measured values of wet film thickness. It is apparent that, as wet film thickness increases, the standard deviation of the replicates also increases. Recall that position "0" along the ROI represents the leading edge of the wet film, while positions around 18 mm and 20 mm are those areas into which drainage of solution from above occurs. This represents another artifact of the dipping simulator; in capsule manufacture, immediately upon completion of the withdrawal steps, the pins are rotated into the dome-upward position and any drainage would be toward the leading edge. The results in Fig. 7 emphasize that we cannot exceed the pixel resolution that arose as a result of our selected dynamic range, and that drainage effects will influence the reproducibility of experiments.

Experiments confirmed that wet film thickness increased as withdrawal speed increased, and clearly demonstrated that insertion speed was of negligible consequence. As expected, it was found that Eq. (2) was unable to predict accurately the behavior of wet film on dipped pins at room temperature.

Thermally Gelling Systems

Experiments in the previous section confirmed the lack of a suitable model to describe dip coating with highly viscous, non-gelling polymer solutions. It was anticipated from the outset of this investigation that dip coating with thermally gelling systems would be even less well described by theories that had been derived from studies of newtonian liquids. Table 4 lists some of the experiments that were performed and also includes trend-line parameters and correlation coefficients of the experimental results. Columns 11–20 list wet film thicknesses, in micrometers, calculated according to the trend-line parameters of columns 7 and 8. Note that all experiments used pin

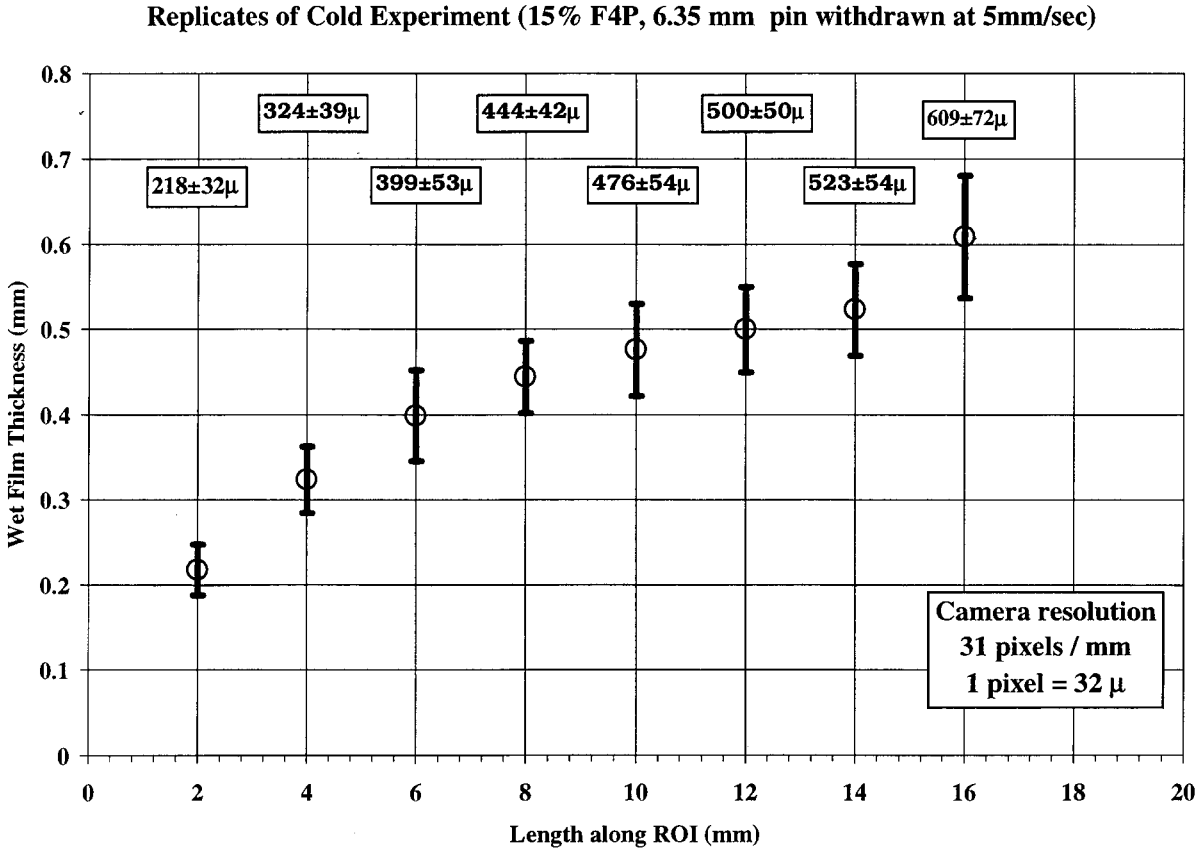

Figure 7. Reproducibility of the video analyses of wet film profiles.

Table 4

Hot Pin Experimental Program and Trend-Line Analyses

1	4	5	6	7	8	9		11	12	13	14	15	16	17	18	19	20
				$y=Ax^b$				EXPERIMENTAL TRENDS									
	SOLN %	PIN C	DELAY SEC	A	b	R^2		x=	2	4	6	8	10	12	14	16	18
47b	20	50	0	0.18	0.54	0.972		y=	260	378	471	550	621	686	745	801	854
48b	20	60	0	0.18	0.52	0.977		y=	256	366	451	523	587	645	698	748	795
49b	20	70	0	0.21	0.50	0.987		y=	296	419	513	593	664	727	786	840	892
44	15	50	0.25	0.21	0.39	0.982		y=	279	366	429	480	524	563	598	630	659
45	15	60	0.25	0.24	0.37	0.975		y=	303	391	454	505	548	586	620	651	680
40a	15	70	0.25	0.18	0.46	0.980		y=	249	341	411	468	519	564	605	643	679
42A	17	50	0.25	0.16	0.47	0.979		y=	224	311	377	432	480	523	563	600	634
43A	17	60	0.25	0.15	0.48	0.980		y=	209	292	354	407	453	494	532	567	600
46	17	70	0.25	0.19	0.39	0.973		y=	243	319	374	419	457	491	521	549	575
47	20	50	0.25	0.20	0.47	0.962		y=	281	390	473	541	602	656	705	751	794
48	20	60	0.25	0.23	0.54	0.987		y=	329	477	593	692	780	860	934	1,004	1,069
49	20	70	0.25	0.17	0.55	0.989		y=	256	374	468	548	620	686	746	803	857
50	15	50	0.5	0.23	0.35	0.963		y=	293	374	432	478	517	551	582	610	635
51	15	60	0.5	0.13	0.56	0.948		y=	188	277	347	408	462	511	557	600	641
52	15	70	0.5	0.15	0.51	0.947		y=	211	300	369	427	478	524	567	607	644
53	17	50	0.5	0.13	0.56	0.973		y=	188	277	347	407	460	509	555	598	638

x = length along ROI, mm y = wet film thickness, μm

diameter 6.35 mm, insertion speed 20 mm/sec, and withdrawal speed 20 mm/sec, except for the final 2 mm of withdrawal length which was withdrawn at 5 mm/sec. It was anticipated that by increasing the thickness at the leading edge, stripping from the pins would be facilitated. Inclusion of various delay times in this experimental program was intended to address this effect; it was proposed that a delay step at maximum insertion would increase the extent of thermal gelation at the leading edge, as shown in Fig. 3.

Illustrative composite plots of a selection of experimental findings are given in Figs. 8–10. In all plots, experiment numbers are shown either in the legend or in the field of the plot. Experiment numbers correspond with those given in the left column of Table 4. All plots show experimental values as opposed to trend-line calculated values.

Figure 8 illustrates that there was no conclusive thickening of the leading edge as a result of having a delay step at maximum depth. Experiments also revealed that wet film profiles were very similar from 50 to 70°C. Figure 9 illustrates the influence of pin temperatures on 15% Methocel™ F4P cellulose ether solutions. For comparison, the plot also includes a wet film profile obtained by dipping an unheated pin into the solution. Heated and unheated dip profiles were not directly comparable; it must be borne in mind that there was no delay step with the unheated pin. The unheated dip profile exhibited significantly more drainage along the

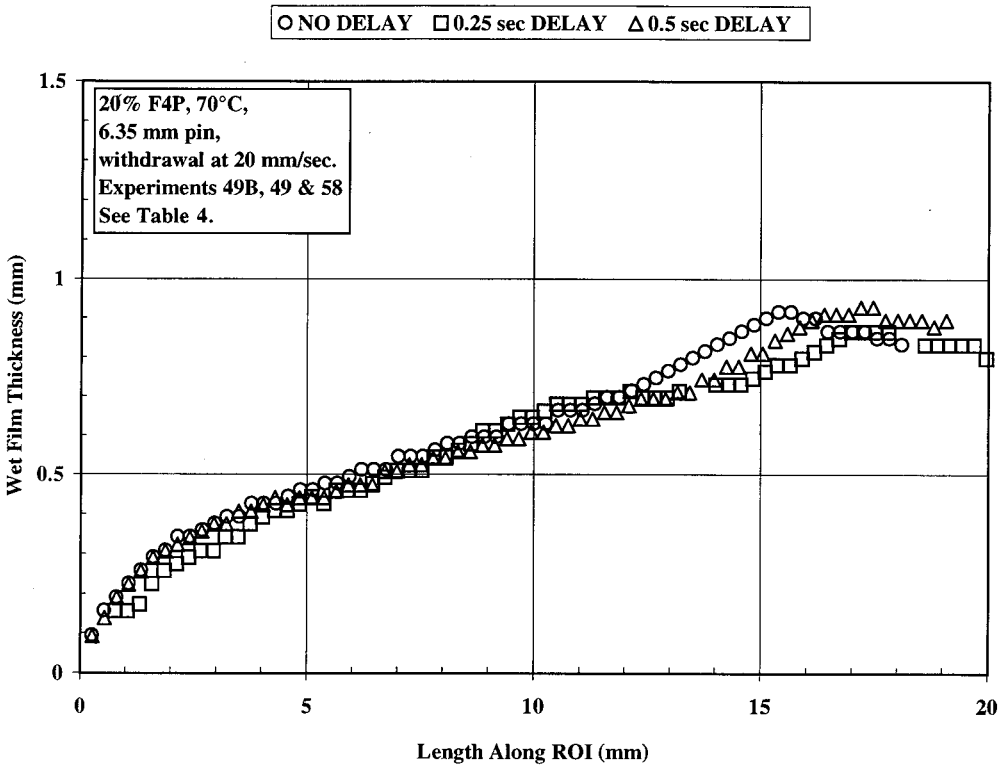

Figure 8. Influence of delay period on wet film profile for pin at 70°C.

length of the ROI than was shown by the heated dip profiles. The remarkably similar results for the elevated temperatures suggested that temperature was of relatively minor importance in comparison to the influence of concentration. Concentration effects were studied, as illustrated in Fig. 10. At temperatures of 50, 60, and 70°C, profiles for 15% and 17% were similar and were significantly different from the profile for 20% F4P.

DISCUSSION

The infinite variety of practical dip sequences, solution concentrations, formulations, and temperatures suggested that a statistically-designed experimental program should have been performed. That this was not done was a result of an ongoing evaluation of "effort vs. return." It was appreciated at the outset of the work that the experimental apparatus could never duplicate the real-world situation. Quite simply, the dynamic mass of air, liquids, and vapors that contributes to the ambient conditions of temperature and humidity during capsule manufacture could never be adequately simulated in a bench-top experiment.

Comparisons of the trends in Table 4 with predictions from Eq. (2) failed to find a satisfactory agreement between experimental trends and theoretical predictions. For the work with heated pins, it was expected that it would be necessary to modify Eq. (2) to accommodate some aspects related to experimental temperatures. Initially, it was anticipated that gel point, or storage modulus at a given temperature, or yield stress at a given temperature would prove to be a relevant component to any model; these could not be demonstrated despite significant effort.

Finally, Eq. (2) was modified empirically, as follows:

$$h = K\sqrt{\frac{\mu x}{\rho g t'}} \tag{5}$$

where K is a variable that is a function of concentration; $K = 0.6$ for 20%, $K = 0.65$ for 17%, $K = 1$ for 15% F4P and t' is the time since the leading edge left the surface of the dip tank minus any delay period.

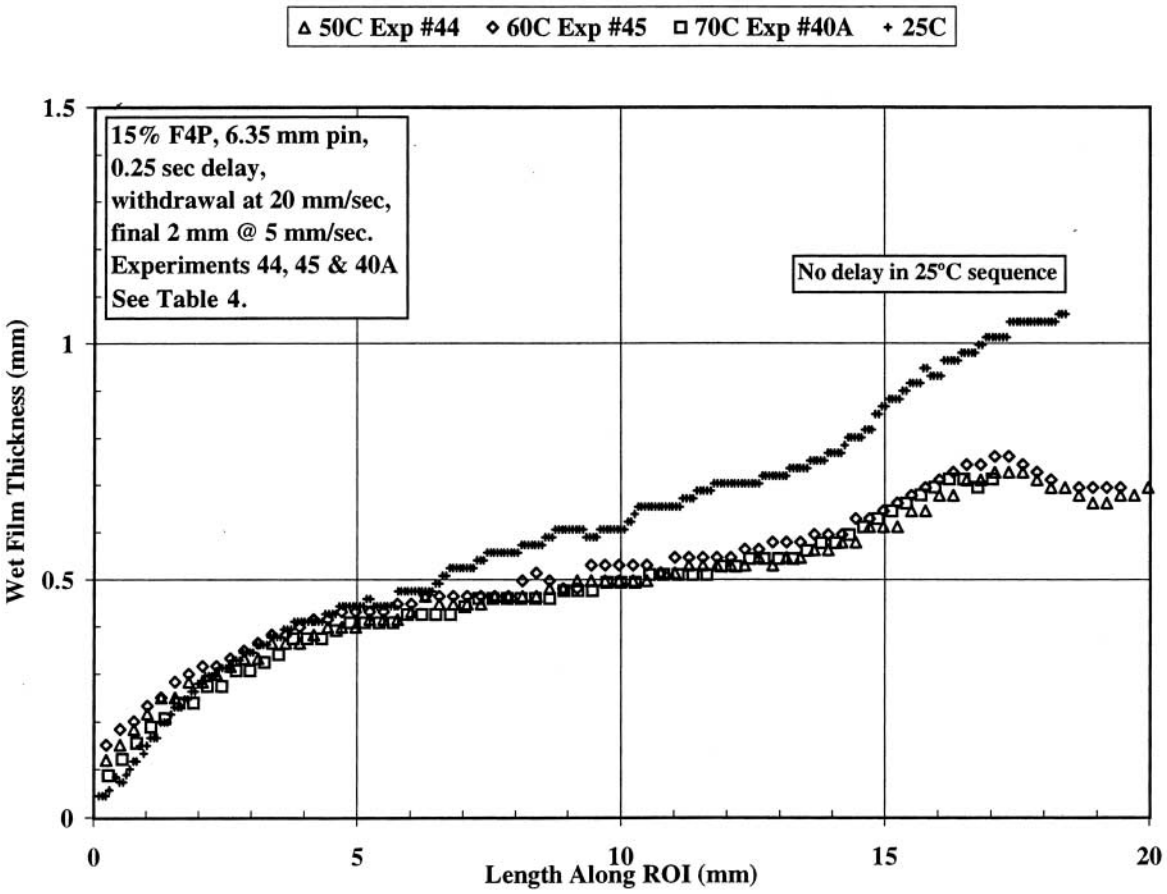

Figure 9. Influence of pin temperature on wet film profile for 15% F4P.

Table 5 lists calculated viscosity and density values used to generate the model data in Table 6. All other terms as used in Eq. (2). Columns 34–42 of Table 6 list the percentage difference between wet film thickness as calculated from $y = Ax^b$ and the thickness calculated from Eq. (5). A positive value in these columns indicates that Eq. (5) predicted values less than the experimental trend. Conversely, a negative value in columns 34–42 would indicate that Eq. (5) predicted values greater than the experimental trend.

A superficial examination of columns 34–42 of Table 6, reveals that, in the majority of cases, Eq. (5) predicted wet film thickness remarkably well. Generally, the greatest absolute differences between experimental trend and model prediction were found closest to the strip edge, i.e., at $x = 2$ mm along the ROI, where the film would be thinnest. Percentage differences between experimental trends and predicted values were generally smaller than those obtained for cold pin experiments.

The Physical Significance of Eq. (5)

Equation (5) was developed by modifying Eq. (2) and the modification was simply to decrease the predicted wet film thickness, h, by a factor whose value depended upon the concentration of the HPMC solution. Figure 3 illustrated a conceptual wet film system proposed as resulting from dipping a heated pin into a HPMC solution. The dimensions of zones 1 and 2 were unknown and remain intractable without recourse to magnetic resonance imaging techniques (MRI), which were not readily available. Dimensional analyses were performed on the withdrawn, coated systems, therefore the video technique yielded a combined thickness measurement for the thermal gel(s) and the adhering viscous liquid.

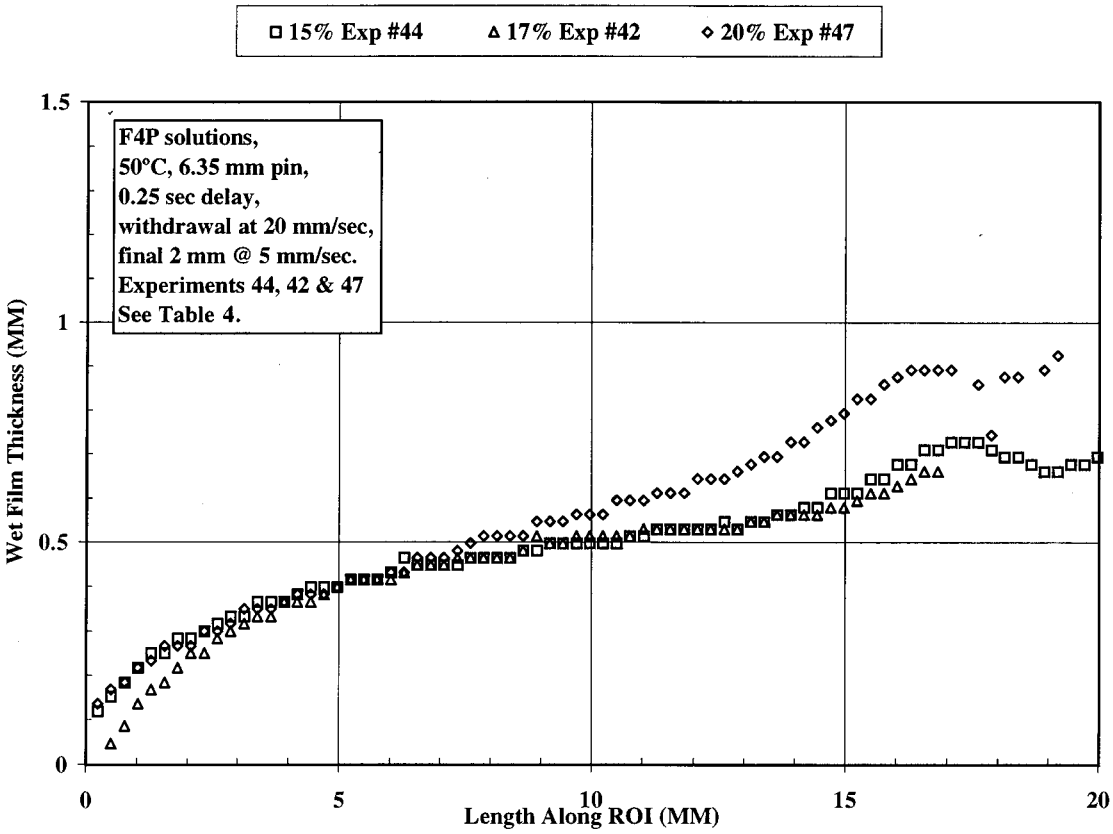

Figure 10. Influence of concentration on wet film profile for pin at 50°C.

Table 5

Calculated Viscosity and Density Values

%	Viscosity (poise)		Viscosity (pa sec)	ρ (g/cm^3)
15	11.9	=	1.19	1.0375
17	21.5	=	2.15	1.0427
20	49	=	4.9	1.0504

For pin temperatures that exceed the gel temperature of the dipping solution by at least 20°C, wet film thickness is relatively independent of temperature:

- within the first 5 sec from the start of withdrawal of the pin;
- for identical pin motions;
- for pin temperatures that do not cause melting or syneresis of the gel;
- for a given HPMC concentration and formulation.

Equation (5) also contains a term, t' which is the time since the leading edge left the surface of the dip tank minus any delay period. The impact of subtracting the delay period is to increase the wet film thickness, calculated by Eq. (5), for those dip sequences that involved a delay step at maximum dip depth. This proposal was not fully supported by experimental evidence, and certainly contributed to the differences that have been reported in Table 6.

In addition to the complexity that the delay step introduced, the withdrawal portion of the cycle involved two steps, as described previously. In capsule manufacture, pins are rotated into a dome-up position upon clearing the surface of the dip liquid. This aspect was not studied in the present program. Consequently, there was often a thickening of wet film around the shoulder of the pins, due to drainage, and this has simply been ignored in the present dimensional analyses. Opinions vary as to the merit of whether or not the pins should have

Table 6

Comparison of Experimental Trends and Predictions from Eq. (5)

1	4	5	21	22	23	24	25	26	27	28	29	30	31	33	34	35	36	37	38	39	40	41	42
															% DIFFERENCE								
								$h=K\sqrt{\frac{\mu x}{\rho g t'}}$							$\left(\frac{Trend-Model}{Trend}\right)\times 100$								
	SOLN %	PIN C	t=	x=	2	4	6	8	10	12	14	16	18	x=	2	4	6	8	10	12	14	16	18
47b	20	50	4.5	h=	276	390	478	552	617	676	730	781	828		-6	-3	-1	0	1	1	2	3	3
48b	20	60	4.5	h=	276	390	478	552	617	676	730	781	828		-8	-7	-6	-5	-5	-5	-5	-4	-4
49b	20	70	4.5	h=	276	390	478	552	617	676	730	781	828		7	7	7	7	7	7	7	7	7
44	15	50	4.5	h=	235	332	406	469	525	575	621	664	704		16	9	5	2	0	-2	-4	-5	-7
45	15	60	4.5	h=	235	332	406	469	525	575	621	664	704		23	15	11	7	4	2	0	-2	-4
40a	15	70	4.5	h=	235	332	406	469	525	575	621	664	704		6	3	1	0	-1	-2	-3	-3	-4
42A	17	50	4.5	h=	205	289	354	409	457	501	541	579	614		9	7	6	5	5	4	4	4	3
43A	17	60	4.5	h=	205	289	354	409	457	501	541	579	614		2	1	0	-1	-1	-1	-2	-2	-2
46	17	70	4.5	h=	205	289	354	409	457	501	541	579	614		16	9	5	2	0	-2	-4	-5	-7
47	20	50	4.5	h=	284	402	492	568	635	696	751	803	852		-1	-3	-4	-5	-6	-6	-7	-7	-7
48	20	60	4.5	h=	284	402	492	568	635	696	751	803	852		14	16	17	18	19	19	20	20	20
49	20	70	4.5	h=	284	402	492	568	635	696	751	803	852		-11	-7	-5	-4	-2	-1	-1	0	1
50	15	50	4.5	h=	242	342	419	484	541	593	640	684	726		18	9	3	-1	-5	-8	-10	-12	-14
51	15	60	4.5	h=	242	342	419	484	541	593	640	684	726		-29	-24	-21	-19	-17	-16	-15	-14	-13
52	15	70	4.5	h=	242	342	419	484	541	593	640	684	726		-15	-14	-14	-13	-13	-13	-13	-13	-13
53	17	50	4.5	h=	211	298	365	422	471	516	558	596	632		-12	-8	-5	-4	-2	-1	-1	0	1
54	17	60	4.5	h=	211	298	365	422	471	516	558	596	632		-11	-11	-11	-11	-11	-11	-11	-11	-11
55	17	70	4.5	h=	211	298	365	422	471	516	558	596	632		12	11	10	9	9	8	8	8	7
56	20	50	4.5	h=	293	414	507	585	655	717	774	828	878		-10	-6	-4	-3	-2	-1	0	1	1
57	20	60	4.5	h=	293	414	507	585	655	717	774	828	878		-28	-13	-6	0	3	6	9	11	13
58	20	70	4.5	h=	293	414	507	585	655	717	774	828	878		-2	-2	-2	-2	-2	-2	-2	-2	-2

x = length along ROI, mm h = wet film thickness, μm

t = time since leading edge left surface of dip tank, sec

t' = t- any delay time, sec

been rotated in the present studies. Preliminary experimental evidence suggested that significant loss of focus upon rotation created such a scatter of results that it was decided not to expend effort on the problem. Also, in capsule manufacturing, the space above the dip tanks achieves a very high humidity and a much higher temperature than could be achieved conveniently with the simulator.

Despite the obvious limitations of the simulator and experimental variability, it was decided to evaluate the ability of Eq. (5) to predict wet film thickness. The results are given in Fig. 11 for a study involving a "real" pin that was supplied by a capsule manufacturer. The pin was tapered and equipped with rings and notches, it was also of a different steel from the simulator pins. Differences between wet film thicknesses from the experimental trend and the predictions of Eq. (5) were less than 11% in every case.

CONCLUSIONS

By simulation and analysis of a dipping process for making hard-shell HPMC capsules it has been

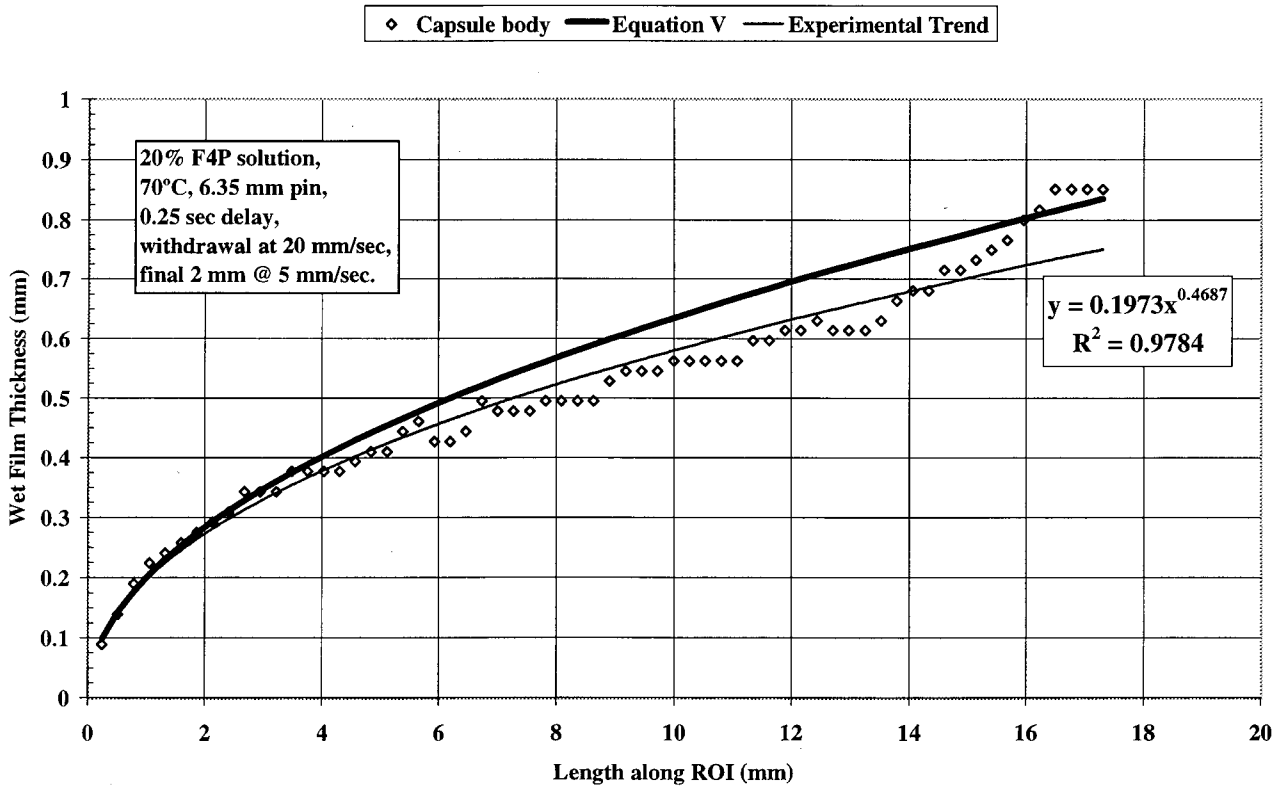

Figure 11. Using Eq. (5) to predict wet film thickness on size "0" body pin.

found that pin temperature plays a minor role in comparison to the effects of solution concentration. The study has demonstrated a limited ability to predict wet film thickness during a hot-pin, cold-solution dipping process. Slight modifications to existing theories were able to accommodate the few experimental variables reported here.

Use of digital video techniques, or optical microscopy, as the basis of a real-time, feedback-controlled system for capsule manufacture appears feasible, but cost analysis would be crucially important. The techniques might also be used, for example, to monitor pin wear, lubricant thickness, progress of drying, and dry film dimensions at any region of the pin.

ACKNOWLEDGMENTS

The authors thank The Dow Chemical Company for permission to publish this article. We also wish to thank Mr. Craig McGraw and Mr. Gary Wright of The Dow Chemical Company for significant contributions to this study, and Daryl Dacko for assistance with the motor control hardware.

REFERENCES

1. Ridgway, K., Ed. *Hard Capsules. Development and Technology*; The Pharmaceutical Press: London, 1987.
2. Grosswald, R.R. et al. Method and Apparatus for the Manufacture of Pharmaceutical Cellulose Capsules. EP 0587773B1, 1992.
3. Sarkar, N. Pharmaceutical Capsules from Improved Thermogelling Methylcellulose Ethers. U.S. Patent 4,001,211, 1977.
4. Scriven, L.E. Physics and Applications of Dip Coating and Spin Coating. Mater. Res. Soc. Symp. Proc. **1988**, *121*, 717–729.
5. Guglielmi, M.; Zenezini, S. The Thickness of Sol–Gel Silica Coatings Obtained by Dipping. J. Non-Cryst. Solids **1990**, *121*, 303–309.

6. Strawbridge, I.; James, P.F. The Factors Affecting the Thickness of Sol–Gel Derived Silica Coatings Prepared by Dipping. J. Non-Cryst. Solids **1986**, *86*, 381–393.
7. Brinker, C.J.; Frye, G.C.; Hurd, A.J.; Ashley, C.S. Fundamentals of Sol–Gel Dip Coating. Thin Solid Films **1991**, *201*, 97–109.
8. Tanguy, P.; Fortin, M.; Choplin, L. Finite Element Simulation of Dip Coating, 1: Newtonian Fluids. Int. J. Num. Meth. Fluids **1984**, *4*, 441–457.
9. Spiers, R.P.; Subbaraman, C.V.; Wilkinson, W.L. Free Coating of a Newtonian Liquid onto a Vertical Surface. Chem. Eng. Sci. **1974**, *29*, 389–396.
10. Spiers, R.P.; Subbaraman, C.V.; Wilkinson, W.L. Free Coating of Non-Newtonian Liquids onto a Vertical Surface. Chem. Eng. Sci. **1975**, *30*, 379–395.
11. Tanguy, P.; Chopin L.; Fortin, M. Shear-Thinning Effects on Dip Coating. Can. J. Chem. Eng. **1985**, *63*, 533–538.
12. Groenveld, P. AIChE J. **1971**, *17*(2), 489–490.
13. Sarkar, N. Kinetics of Thermal Gelation of Methylcellulose and Hydroxypropyl Methylcellulose in Aqueous Solutions. Carbohydr. Polym. **1994**, *24*, 1–9.
14. Haque, A.; Morris, E.R. Thermogelation of Methylcellulose. Part I: Molecular Structures and Processes. Carbohydr. Polym. **1993**, *22*, 161–173.
15. Haque, A.; Richardson, R.K.; Moris, E.R.; Gildey, M.J.; Caswell, D.C. Thermogelation of Methylcellulose. Part II: Effect of Hydroxypropyl Substituents, Carbohydr. Polym. **1993**, **22**, 175–186.